Release of Halide Ions from the Buried Active Site of the Haloalkane Dehalogenase LinB Revealed by Stopped-Flow Fluorescence Analysis and Free Energy Calculations

Jana Hladilkova,[1] Zbynek Prokop,[2] Radka Chaloupkova[2], Jiri Damborsky[2], and Pavel Jungwirth[1*]

[1]Institute of Organic Chemistry and Biochemistry, Academy of Sciences of the Czech Republic, Flemingovo nam. 2, 16610 Prague 6, Czech Republic and [2]Loschmidt Laboratories, Department of Experimental Biology and Research Centre for Toxic Compounds in the Environment, Faculty of Science, Masaryk University, Kamenice 5/A13, 625 00 Brno, Czech Republic.

*Corresponding author: pavel.jungwirth@uochb.cas.cz

Keywords: Access tunnel; buried active site; catalytic activity; enzyme mechanism; haloalkane dehalogenase; halide ions

Abstract

Release of halide ions is an essential step of the catalytic cycle of haloalkane dehalogenases. Here we describe experimentally and computationally the process of release of a halide anion from the buried active site of the haloalkane dehalogenase LinB. Using stopped-flow fluorescence analysis and umbrella sampling free energy calculations we showed that the anion binding is ion-specific and follows the ordering $I^- > Br^- > Cl^-$. We have also addressed the issue of the protonation state of the catalytic His272 residue and its effect on the process of halide release. While deprotonation of His272 increases binding of anions in the access tunnel, we showed that the anionic ordering does not change with the switch of the protonation state. We also demonstrated that a sodium cation could relatively easily enter the active site, provided the His272 residue is singly protonated, and replace thus the missing proton. In contrast, Na^+ is strongly repelled from the active site containing the doubly protonated His272 residue. Our study contributes towards understanding of the reaction mechanism of haloalkane dehalogenase enzyme family. Determination of the protonation state of the catalytic histidine throughout the catalytic cycle remains a challenge for future studies.

Introduction

Haloalkane dehalogenases are hydrolytic enzymes that catalyze the cleavage of the carbon-halogen bonds in a broad range of halogenated hydrocarbons. The reaction mechanism of these enzymes has been extensively studied by protein crystallography [1-10], enzyme kinetics [2, 11-15], and molecular modelling[16-30]. The catalytic cycle of these enzymes consists of following steps: (i) substrate binding, (ii) nucleophilic substitution reaction leading to formation of a halide ion and an alkyl-enzyme intermediate, (iii) nucleophilic addition reaction leading to formation a primary alcohol and a proton, and (iv) products (an alcohol, a halide, and a proton) release. The individual steps of the catalytic cycle are balanced and the rate-limiting step can be different for individual enzyme-substrate pairs, ranging from limitation at the nucleophilic substitution, through hydrolysis of the alkyl-enzyme intermediate, to an alcohol or a halide ion release [12]. Substrate binding remains the only step of the catalytic cycle, which is fast in every studied enzyme and does not limit the overall catalytic cycle of kinetically characterized haloalkane dehalogenases. The catalytic triad (nucleophilic Asp - catalytic base His - catalytic acid Asp/Glu) and two halide-stabilising residues (Trp-Trp or Trp-Asn) are directly involved in the catalysis. The catalytic histidine changes its protonation state during the catalytic cycle, but the exact fate of the proton abstracted from the catalytic water is not known. The mechanism of halide ion solvation by the water molecules accessing the active site and their release via protein tunnels also remains elusive [15, 23, 31, 32].

In our previous study, we have investigated specific cationic interactions at the tunnel mouth and their effects on the enzymatic activity of wild type LinB and its mutants [33]. Three of the present authors also participated in an exploratory study of the effect of tunnel mutation on the release of a bromide anion as one of the products of the enzymatic process [34]. The principal aim of the present study is three fold. First, we employ the stopped-flow fluorescence analysis and free energy umbrella sampling simulations to determine ordering of halide anions Cl^-, Br^-, and I^- according to their free energies of binding in the active site tunnel of LinB. Second, we explore the protonation state of the catalytic His272 residue and its effect on halide binding. Third, we investigate whether a sodium cation could accommodate in the active site in the case of singly protonated His272.

Experimental and Computational Methods

Stopped-Flow Fluorescence Analysis - Experiments were performed with the stopped-flow instrument SFM-300 combined with the spectrometer system MPS-200 equipped with a Xe (Hg) lamp (BioLogic, France) with excitation at 295 nm. Fluorescence emission from Trp residues was observed through a 320 nm cut-off filter supplied with the instrument. All reactions were performed at 37°C in 100 mM glycine buffer pH 8.6. Association equilibrium constant of specific binding (K_{as}), apparent association equilibrium constant of the non-specific quenching interaction (K_Q), and the relative fluorescence intensity of enzyme-halide complex (*f*) were calculated using Stern-Volmer equation from the amplitudes of fluorescence quench observed upon binding of individual halides (eq. 1). Data fitting was performed using the software Origin 6.1 (OriginLab, USA). The free energy of binding (ΔG_{as}) was calculated from the specific binding constant using the Gibbs free energy formula $\Delta G_{as} = -RT\ln K_{as}$.

$$F / F_0 = \frac{1}{1 + K_Q [X^-]} \cdot \frac{1 + f \cdot K_{as} [X^-]}{1 + K_{as} [X^-]} \qquad (1)$$

Simulated System – The crystal structure of the wild type LinB dehalogenase (PDB code 1MJ5) [35] was adopted and solvated in a periodic unit cell containing ~11000 water molecules, which includes both crystal structure and additionaly placed bulk water molecules. We considered both possible protonation states of the catalytic histidine (His272) as it can change during the enzymatic cycle [36] and so far remains uncertain: His272 protonated on both nitrogen atoms (= charged) or singly protonated His272 at the N_δ atom (= neutral). The total charge of the enzyme was consequently -10 e in the first case or -11 e in the second case. This extra charge was compensated by additional cations, which were of the same origin as from the added 0.5 M salt (100 alkali cations and 100 halide anions). The parameterization of the ions was the same as in our earlier studies [37], which proved to be a reliable choice in combination with the ff03 protein force field [38] and the SPC/E water model [39].

Classical Molecular Dynamics (MD) Simulations – All calculations were carried out using the Amber 11 program package [40] according to the simulation protocol used in our previous protein studies [33, 37]. The potential energy of the system was first minimized with constrained positions of protein atoms using the steepest descent method to avoid unfavorable close contacts. The system was then slowly heated up to 300 K with volume held fixed and, subsequently, pressure coupling was employed to reach the equilibrium density. After 2 ns equilibration the data were collected from the subsequent 10-30 ns production runs. All bonds involving hydrogen atoms were constrained using the SHAKE algorithm [41], allowing for a 2 fs timestep. The short range non-bonded interactions were cut off at 9 Å and smooth particle mesh Ewald (PME) method accounted for the long range electrostatics [42]. The Berendsen's pressure and temperature coupling schemes (with coupling frequency of 1 ps^{-1}) were employed [43].

Free Energy Profiles – Free energy profiles of all ions were calculated using the umbrella sampling procedure [44]. The target distance in every window was measured from the center of the N(Asn38) – N(Trp109) segment of the halide-stabilizing residues to the ion. To avoid problems with shifting of the origin of the umbrella sampling, these two residues were constrained during the whole procedure. For every window, separated by 0.5 Å from the previous one, the simulation lasted for 12 ns. In total, 52 windows were simulated for each ion (Cl^-, Br^-, I^-, or Na^+) in the LinB tunnel for both protonated and neutral catalytic His272 residue. In total, 5.0 μs of data were analyzed by the WHAM [44]. This procedure, however, does not include a volume entropy correction due to the use of a non-Cartesian coordinate. A simple r^2 correction pertinent to a radial coordinate is not adequate since the tunnel size restricts the angular movements of the ion. Therefore, we had to calculate the accessible volume for the ion in each window and perform a manual correction using the following formula:

$$F^{REAL} = F^{WHAM} + kT \times \frac{\ln(V)}{4185} \qquad (2)$$

Results

Stopped-flow fluorescence experiments were used to establish the kinetics of halide binding using the intrinsic tryptophan fluorescence of LinB. Binding of all tested halides to haloalkane dehalogenase LinB showed rapid establishment of equilibrium; the fluorescence quench occurred in the dead time of the instrument (2 ms) and only steady-state fluorescence was observed (Figure 1). In all cases, the dependence of relative fluorescence on halide concentration (Figure 2) showed strong quenching activity at lower halide concentrations (0 – 500 mM), suggesting specific binding of a halide ion to the LinB active site associated with its strong interaction with the halide stabilizing tryptophan (K_{as}). A weak non-specific quenching was observed at high concentration of halides suggesting non-specific interactions with other tryptophans outside of the active site (K_Q). The experimental equilibrium constants for chloride, bromide, and iodide binding to LinB are summarized in Table 1. The resulting binding free energy values (ΔG_{as}) order the halides as $I^- >> Br^- > Cl^-$.

Next, we addressed halide binding to LinB by MD simulations. In the beginning of the 20 ns simulation runs a halide anion was put in five different positions close to the halide stabilizing residues of LinB active site and its exit pathway was followed. In all cases and for all investigated anions – Cl^-, Br^- and I^-, the result was the same. Namely, the anion left the active site through the p1b tunnel (see Fig. 3), which is in a qualitative agreement with a previous computational studies [23, 32].

In order to investigate differences between the behavior of the halide ions, free energy profiles of Cl^-, Br^- and I^- were calculated using the umbrella sapling method. The origin of the reaction path was taken as the average position between the nitrogen atoms of the halide-stabilizing residues ($Asn38_{N\delta2}$ and $Trp109_{N\varepsilon1}$). The distance between the origin and the halide was then increased in every window by 0.5 Å until the halide anion reached the aqueous bulk region. In the post-processing procedure, the applied biased force was subtracted and the volume entropy correction, described above, was applied.

The resulting free energy profiles for the three investigated halide anions are depicted, for the case of a doubly protonated catalytic His272 residue, in Fig. 2. Qualitatively, the three profiles have similar shapes. The first and at the same time deepest minimum along the reaction path is located 2.2 Å, 2.4 Å or 2.7 Å from the origin for Cl^-, Br^- or I^-, respectively. It reflects interactions with the ion-

stabilizing residues Asn38 and Trp109 with binding free energies ΔG_{min} in the order $I^- \geq Br^- >> Cl^-$. The main barrier on the free energy curve is situated at 4.1 Å and its height practically coincides for all three anions. However, upon closer inspection of the simulations, rather than localized ion positions at the barrier we find a flat region perpendicular to the reaction coordinate, where anions move relatively freely, as schematically shown in Fig. 5. Behind the barrier, we observe a secondary minimum about 6-8 Å from the origin, i.e., close to the catalytic His272, which stabilizes anions in following order: $I^- > Br^- > Cl^-$. All the halide anions reach the p1b tunnel mouth at ~12-13 Å and move then freely into the aqueous bulk region. From the opposite direction, the initial barrier to enter into the tunnel is 4-6 kcal/mol, being the lowest for iodide, followed by bromide and chloride. The schematic anionic path through the tunnel is depicted in Fig. 5. The value, which is directly comparable to the experimentally measured ΔG_{as}, is estimated as the ΔG_{min}, corresponding to the deepest minimum on the calculated free energy path (Fig. 4). For I^- and Br^- the stabilization of the anion is stronger close to the halide-stabilizing residues than in the bulk solution (ΔG_{as} ~ -0.5 kcal/mol), the opposite being true for Cl^- with ΔG_{as} = +1.0 kcal/mol (Table 2).

In the case of LinB with a singly protonated catalytic His272 residue, the resulting free energy profiles of all halides have again similar shapes, however, they differ from those in the case of doubly protonated His272 (compare Fig. 4 and Fig. 6). The first minima are located at the same distances as in the previous case but are deeper and the ordering of ion in terms of their stabilization is slightly more pronounced: $I^- > Br^- >> Cl^-$. Simulations show that average hydration of the anions between the halide-stabilizing residues slightly decreases upon deprotonation of His272, which indicates their better embedding in this case. This is true in particular for the most strongly bound iodide anion, which readily sheds off a water molecule when binding to the halide-stabilizing residues.

The whole region around the first maximum on the free energy profiles also differs for the two protonation cases since the catalytic triad (Asp108, His272, and Glu38) changes its conformation once the His272 becomes only singly protonated (Figs. 4 and 6). Conformational changes of Asp108 side-chain has been observed in the high-resolution structure of LinB [35]. On top of that, there is no more anion-stabilizing effect close to the singly protonated His272, therefore, we now observe roughly plateau regions at around the distance of 8 Å (Fig. 6) instead of the pronounced secondary minima in

the case of doubly protonated His272 (Fig. 4). By deprotonation of His272 the maximum of the free energy curves becomes shifted to the p1b tunnel mouth (~12-13 Å) and the barrier for anion to enter into the tunnel increased to 6-7.5 kcal/mol (compare Fig. 4 and Fig. 6). The representative path of the anion through the tunnel is schematically depicted in Fig. 8. For the case of singly protonated His272, we observe stronger stabilization of all the anions close to the active site than in the bulk solution by 0.6-2.1 kcal/mol, as summarized in Table 2.

The uncertainty of the protonation state of His272 at the active site implies yet another question. Can in principle the negative charge be compensated instead of a proton by an alkali cation or is it improbable for cation to enter into the active site? Within the crystal structures there was no explicit cation observed at the active site, however, a sodium cation can be easily misinterpreted as a water molecule. Therefore, we calculated the free energy profile also for a sodium cation, assuming either of the two protonation states of His272. When His272 is doubly protonated we observe no stabilization of the sodium cation at any place in the whole tunnel (Fig. 9), despite the fact that the overall charge of the active site is still negative (-1 e). Upon deprotonation of His272 the overall charge at the active site becomes -2 e and, consequently, we observe a local minimum for the sodium cation between Asp108 and His272 (Fig. 9). The way how sodium is released from the active site is similar to that for the anions (Fig. 8), however, the barrier to enter into the p1b tunnel becomes significantly lower (~3 kcal/mol). Nevertheless, even for the case of deprotonated His272 sodium prefers bulk solution over the active site by almost 2 kcal/mol. This is an opposite behavior to the halide anions with specific binding partners at the tunnel bottom.

Discussion

The present joint experimental and computational study has established the binding order $I^- > Br^- > Cl^-$ of heavier halides in the active side of the haloalkane dehalogenase LinB. Part of the reason iodide binds the strongest is that the geometry and electrostatics of the site formed by the halide-stabilizing residues allows it to easily shed off a water molecule and replace it by binding to the halide-stabilizing residues. In contrast, the hydration shell of chloride is too tight to allow for this easy swapping of a binding partner, which results in the weakest binding energy among the investigated anions. For

bromide, which lies in the middle between I^- and Cl^-, this study involving converged simulation times and a proper account for the volume entropy correction also represents a refinement of earlier calculations [34].

Comparison between the experimental and calculated binding free energies of the halide anions should in principle allow us to determine the protonation state of the catalytic His272 residue during the product release step. Unfortunately, the ordering of the halides is the same for the two protonation states and the corresponding differences between the binding energies are comparable to the estimated accuracy of ±1 kcal/mol of the calculated free energies. Therefore, we are currently exploring possibilities of determining the protonation state of His272 during the catalytic cycle using NMR spectroscopy. Due to the presence of multiple titratable histidines in LinB, this may, however, turn out to be a "needle in a haystack" problem.

We have also addressed the issue of a potential presence of a sodium cation in the active site, in order to compensate the missing positive charge of the singly protonated His272 residue. Based on the simulations, we cannot exclude the presence of Na^+ (which could easily be confused with a water molecule in crystallographic studies) in the active site, although the corresponding free energy minimum is very shallow and lies slightly above the free energy of a free aqueous sodium cation. In case of the doubly protonated His272 residue sodium is, however, strongly repelled from the active site.

Conclusions

The structural basis and energetics of the halide ion release from the buried active site was studied by stopped-flow and free energy calculations. The main access tunnel of LinB (p1b) was identified as the most probable route for halide release, which is in good agreement with previous studies [15, 23, 32]. This process is ion-specific and depends on: (i) protonation state of the catalytic histidine lining the access tunnel and (ii) hydration properties of individual ions. For a doubly protonated catalytic histidine, two energy minima were identified for all three studied halide ions, one in between two-halide stabilizing residues and second near this His272. The latter, however, practically disappears when the catalytic histidine is singly protonated. Stabilization of the anion in the active site of LinB

follows the order $I^- > Br^- > Cl^-$ for both protonation states of the catalytic residue His272. The protonation state of the catalytic histidine during the catalytic cycle could not be determined unambiguously by our analysis and must be further studied by NMR spectroscopy or neutron diffraction.

Acknowledgment: P.J. thank the Czech Science Foundation (grant P208/12/G016) for support and the Academy of Sciences for the Praemium Academie award. J.D. acknowledges the Czech Science Foundation (grant P207/12/0775) for support. J. H. is grateful for support from the International Max-Planck Research School for Dynamical Processes in Atoms, Molecules and Solids in Dresden. We would like to express thanks to the technician Hana Moskalikova (Masaryk University) for help with the stopped-flow experiments.

References

1. Verschueren, K. H. G.; Seljee, F.; Rozeboom, H. J.; Kalk, K. H.; Dijkstra, B. W., Crystallographic Analysis of the Catalytic Mechanism of Haloalkane Dehalogenase. *Nature* **1993,** 363, 693-698.

2. Prokop, Z.; Sato, Y.; Brezovsky, J.; Mozga, T.; Chaloupkova, R.; Koudelakova, T.; Jerabek, P.; Stepankova, V.; Natsume, R.; van Leeuwen, J. G. E.; Janssen, D. B.; Florian, J.; Nagata, Y.; Senda, T.; Damborsky, J., Enantioselectivity of Haloalkane Dehalogenases and its Modulation by Surface Loop Engineering. *Angewandte Chemie International Edition* **2010,** 49, (35), 6111-6115.

3. Okai, M.; Ohtsuka, J.; Imai, L. F.; Mase, T.; Moriuchi, R.; Tsuda, M.; Nagata, K.; Nagata, Y.; Tanokura, M., Crystal Structure and Site-Directed Mutagenesis Analyses of Haloalkane Dehalogenase LinB from Sphingobium sp. Strain MI1205. *Journal of Bacteriology* **2013,** 195, 2642-2651.

4. Oakley, A. J.; Klvana, M.; Otyepka, M.; Nagata, Y.; Wilce, M. C. J.; Damborsky, J., Crystal Structure of Haloalkane Dehalogenase LinB from *Sphingomonas paucimobilis* UT26 at 0.96 A Resolution: Dynamics of Catalytic Residues. *Biochemistry* **2004,** 43, (4), 870-878.

5. Newman, J.; Peat, T. S.; Richard, R.; Kan, L.; Swanson, P. E.; Affholter, J. A.; Holmes, I. H.; Schindler, J. F.; Unkefer, C. J.; Terwilliger, T. C., Haloalkane Dehalogenase: Structure of a *Rhodococcus* Enzyme. *Biochemistry* **1999,** 38, 16105-16114.

6. Mazumdar, P. A.; Hulecki, J. C.; Cherney, M. M.; Garen, C. R.; James, M. N., X-ray Crystal Structure of *Mycobacterium tuberculosis* Haloalkane Dehalogenase Rv2579. *Biochimica et Biophysica Acta* **2008,** 1784, (2), 351-362.

7. Marek, J.; Vevodova, J.; Kuta-Smatanova, I.; Nagata, Y.; Svensson, L. A.; Newman, J.; Takagi, M.; Damborsky, J., Crystal Structure of the Haloalkane Dehalogenase from *Sphingomonas paucimobilis* UT26. *Biochemistry* **2000,** 39, 14082-14086.

8. Liu, X.; Hanson, B. L.; Langan, P.; Viola, R. E., The Effect of Deuteration on Protein Structure: A High-Resolution Comparison of Hydrogenous and Perdeuterated Haloalkane Dehalogenase. *Acta Crystallographica D* **2007,** 63, (Pt 9), 1000-1008.

9. Hesseler, M.; Bogdanovic, X.; Hidalgo, A.; Berenguer, J.; Palm, G. J.; Hinrichs, W.; Bornscheuer, U. T., Cloning, Functional Expression, Biochemical Characterization, and Structural Analysis of a Haloalkane Dehalogenase from *Plesiocystis pacifica* SIR-1. *Applied and Environmental Microbiology* **2011,** 91, (4), 1049-1060.

10. Gehret, J. J.; Gu, L.; Geders, T. W.; Brown, W. C.; Gerwick, L.; Gerwick, W. H.; Sherman, D. H.; Smith, J. L., Structure and Activity of DmmA, a Marine Haloalkane Dehalogenase. *Protein Science* **2012,** 21, (2), 239-248.

11. Bosma, T.; Pikkemaat, M. G.; Kingma, J.; Dijk, J.; Janssen, D. B., Steady-State and Pre-Steady-State Kinetic Analysis of Halopropane Conversion by a *Rhodococcus* Haloalkane Dehalogenase. *Biochemistry* **2003,** 42, 8047-8053.

12. Prokop, Z.; Monincova, M.; Chaloupkova, R.; Klvana, M.; Nagata, Y.; Janssen, D. B.; Damborsky, J., Catalytic Mechanism of the Haloalkane Dehalogenase LinB from *Sphingomonas paucimobilis* UT26. *Journal of Biological Chemistry* **2003,** 278, 45094-45100.

13. Schanstra, J. P.; Kingma, J.; Janssen, D. B., Specificity and Kinetics of Haloalkane Dehalogenase. *Journal of Biological Chemistry* **1996,** 271, 14747-14753.

14. Schanstra, J. P.; Janssen, D. B., Kinetics of Halide Release of Haloalkane Dehalogenase: Evidence for a Slow Conformational Change. *Biochemistry* **1996,** 35, 5624-5632.

15. Biedermannova, L.; Prokop, Z.; Gora, A.; Chovancova, E.; Kovacs, M.; Damborsky, J.; Wade, R. C., A Single Mutation in a Tunnel to the Active Site Changes the Mechanism and Kinetics of Product Release in Haloalkane Dehalogenase LinB. *The Journal of Biological Chemistry* **2012,** 287, 29062-29074.

16. Hur, S.; Kahn, K.; Bruice, T. C., Comparison of Formation of Reactive Conformers for the SN2 Displacements by CH3CO2- in Water and by Asp124-CO2- in a Haloalkane Dehalogenase. *Proceedings of the National Academy of Sciences of the USA* **2003,** 100, (5), 2215-2219.

17. Kmunicek, J.; Luengo, S.; Gago, F.; Ortiz, A. R.; Wade, R. C.; Damborsky, J., Comparative Binding Energy Analysis of the Substrate Specificity of Haloalkane Dehalogenase from Xanthobacter Autotrophicus GJ10. *Biochemistry* **2001,** 40, (30), 8905-8917.

18. Damborsky, J.; Kuty, M.; Nemec, M.; Koca, J., A Molecular Modeling Study of the Catalytic Mechanism of Haloalkane Dehalogenase: 1. Quantum Chemical Study of the First Reaction Step. *Journal of Chemical Information and Computer Sciences* **1997,** 37, 562-568.

19. Bohac, M.; Nagata, Y.; Prokop, Z.; Prokop, M.; Monincova, M.; Tsuda, M.; Koca, J.; Damborsky, J., Halide-Stabilizing Residues of Haloalkane Dehalogenases Studied by Quantum Mechanic Calculations and Site-Directed Mutagenesis. *Biochemistry* **2002,** 41, 14272-14280.

20. Lightstone, F. C.; Zheng, Y. J.; Bruice, T. C., Molecular Dynamics Simulations of Ground and Transition States for the S(N)2 Displacement of Cl- from 1,2-Dichloroethane at the Active Site of *Xanthobacter Autotrophicus* Haloalkane Dehalogenase. *Journal of American Chemical Society* **1998,** 120, (23), 5611-5621.

21. Maulitz, A. H.; Lightstone, F. C.; Zheng, Y. J.; Bruice, T. C., Nonenzymatic and Enzymatic Hydrolysis of Alkyl Halides: A Theoretical Study of the S(N)2 Reactions of Acetate and Hydroxide Ions with Alkyl Chlorides. *Proceedings of the National Academy of Sciences of the USA* **1997,** 94, 6591-6595.

22. Nam, K.; Prat-Resina, X.; Garcia-Viloca, M.; Devi-Kesavan, L. S.; Gao, J. L., Dynamics of an Enzymatic Substitution Reaction in Haloalkane Dehalogenase. *Journal of the American Chemical Society* **2004,** 126, (5), 1369-1376.

23. Negi, S. S.; Schein, C. H.; Oezguen, N.; Power, T. D.; Braun, W., InterProSurf: A Web Server for Predicting Interacting Sites on Protein Surfaces. *Bioinformatics* **2007,** 23, (24), 3397-3399.

24. Olsson, M. H.; Warshel, A., Solute Solvent Dynamics and Energetics in Enzyme Catalysis: The S(N)2 Reaction of Dehalogenase as a General Benchmark. *Journal of American Chemical Society* **2004,** 126, (46), 15167-15179.

25. Shurki, A.; Strajbl, M.; Villa, J.; Warshel, A., How Much do Enzymes Really Gain by Restraining Their Reacting Fragments? *Journal of American Chemical Society* **2002,** 124, 4097-4107.

26. Silberstein, M.; Dennis, S.; Brown, L.; Kortvelyesi, T.; Clodfelter, K.; Vajda, S., Identification of Substrate Binding Sites in Enzymes by Computational Solvent Mapping. *Journal of Molecular Biology* **2003,** 332, (5), 1095-1113.

27. Soriano, A.; Silla, E.; Tunon, I., Internal Rotation of 1,2-Dichloroethane in Haloalkane dehalogenase. A Test Case for Analyzing Electrostatic Effects in Enzymes. *Journal of Physical Chemistry* **2003,** 107, 6234-6238.

28. Murugan, N. A.; Agren, H., 1,2-Dichloroethane in Haloalkane Dehalogenase Protein and in Water Solvent: A Case Study of the Confinement Effect on Structural and Dynamical Properties. *Journal of Physical Chemistry B* **2009,** 113, 3257-3263.

29. Sharir-Ivry, A.; Shnerb, T.; Strajbl, M.; Shurki, A., VB/MM Protein Landscapes: A Study of the S(N)2 Reaction in Haloalkane Dehalogenase. *Journal of Physical Chemistry B* **2010,** 114, 2212-2218

30. Negri, A.; Marco, E.; Damborsky, J.; Gago, F., Stepwise dissection and visualization of the catalytic mechanism of haloalkane dehalogenase LinB using Molecular Dynamics Simulations and Computer Graphics. *Journal of Molecular Graphics & Modelling* **2007,** 26, (3), 643-651.

31. Pavlova, M.; Klvana, M.; Prokop, Z.; Chaloupkova, R.; Banas, P.; Otyepka, M.; Wade, R. C.; Tsuda, M.; Nagata, Y.; Damborsky, J., Redesigning Dehalogenase Access Tunnels as a Strategy for Degrading an Anthropogenic Substrate. *Nature Chemical Biology* **2009,** 5, (10), 727-733.

32. Klvana, M.; Pavlova, M.; Koudelakova, T.; Chaloupkova, R.; Dvorak, P.; Prokop, Z.; Stsiapanava, A.; Kuty, M.; Kuta-Smatanova, I.; Dohnalek, J.; Kulhanek, P.; Wade, R. C.; Damborsky, J., Pathways and Mechanisms for Product Release in the Engineered Haloalkane Dehalogenases Explored Using Classical and Random Acceleration Molecular Dynamics Simulations. *Journal of Molecular Biology* **2009,** 392, (5), 1339-1356.

33. Stepankova, V.; Paterova, J.; Damborsky, J.; Jungwirth, P.; Chaloupkova, R.; Heyda, J., Cation-Specific Effects on Enzymatic Catalysis Driven by Interactions at the Tunnel Mouth. *Journal of Physical Chemistry B* **2013,** 117, (21), 6394-6402.

34. Biedermannova, L.; Prokop, Z.; Gora, A.; Chovancova, E.; Kovacs, M.; Damborsky, J.; Wade, R. C., A Single Mutation in a Tunnel to the Active Site Changes the Mechanism and Kinetics of Product Release in Haloalkane Dehalogenase LinB. *Journal of Biological Chemistry* **2012,** 287, (34), 29062-29074.

35. Oakley, A. J.; Klvana, M.; Otyepka, M.; Nagata, Y.; Wilce, M. C. J.; Damborsky, J., Crystal Structure of Haloalkane Dehalogenase LinB from Sphingomonas paucimobilis UT26 at 0.95 Angstrom Resolution: Dynamics of Catalytic Residues. *Biochemistry* **2004,** 43, (4), 870-878.

36. Verschueren, K. H. G.; Seljee, F.; Rozeboom, H. J.; Kalk, K. H.; Dijkstra, B. W., Crystallographic Analysis of the Catalytic Mechanism of Haloalkane Dehalogenase. *Nature* **1993,** 363, (6431), 693-698.

37. Heyda, J.; Kozisek, M.; Bednarova, L.; Thompson, G.; Konvalinka, J.; Vondrasek, J.; Jungwirth, P., Urea and Guanidinium Induced Denaturation of a Trp-Cage Miniprotein. *Journal of Physical Chemistry B* **2011,** 115, (28), 8910-8924.

38. Duan, Y.; Wu, C.; Chowdhury, S.; Lee, M. C.; Xiong, G. M.; Zhang, W.; Yang, R.; Cieplak, P.; Luo, R.; Lee, T.; Caldwell, J.; Wang, J. M.; Kollman, P., A Point-Charge Force Field for Molecular Mechanics Simulations of Proteins Based on Condensed-Phase Quantum Mechanical Calculations. *Journal of Computational Chemistry* **2003,** 24, (16), 1999-2012.

39. Berendsen, H. J. C.; Grigera, J. R.; Straatsma, T. P., The Missing Term in Effective Pair Potentials. *Journal of Physical Chemistry* **1987,** 91, (24), 6269-6271.

40. Case, D. A. D., T. A.; Cheatham, III, T. E; Simmerling, C. L.; Wang, J.; Duke, R. E.; Luo, R.; Walker, R. C.; Zhang, W.; Merz, K. M.; Roberts, B.; Wang, B.; Hayik, S.; Roitberg, A.; Seabra, G.; Kolossvai, K. F.;Wong, F.; Paesani, J.; Vanicek, J.; Liu, J.; Wu, X.; Brozell, S. R.; Steinbrecher, T.; Gohlke, H.; Cui, Q.; Roe, D. R.; Mathews, D. H.; Seetin, M. G.; Sagui, C.; Babin, V.; Luchko, T.; Gusarov, S.; Kovalenko, A.; Kollman, P. A. *AMBER 11*, University of California: San Francisco, 2010.

41. Ryckaert, J. P.; Ciccotti, G.; Berendsen, H. J. C., Numerical-Integration of Cartesian Equations of Motion of a System with Constraints - Molecular-Dynamics of N-Alkanes. *Journal of Computational Physics* **1977,** 23, (3), 327-341.

42. Essmann, U.; Perera, L.; Berkowitz, M. L.; Darden, T.; Lee, H.; Pedersen, L. G., A Smooth Particle Mesh Ewald Method. *Journal of Chemical Physics* **1995,** 103, (19), 8577-8593.

43. Berendsen, H. J. C.; Postma, J. P. M.; Vangunsteren, W. F.; Dinola, A.; Haak, J. R., Molecular-Dynamics with Coupling to an External Bath. *Journal of Chemical Physics* **1984,** 81, (8), 3684-3690.

44. Kumar, S.; Bouzida, D.; Swendsen, R. H.; Kollman, P. A.; Rosenberg, J. M., The Weighted Histogram Analysis Method for Free-Energy Calculations on Biomolecules. 1. The Method. *Journal of Computational Chemistry* **1992,** 13, (8), 1011-1021.

FIGURE LEGENDS

FIGURE 1

Fluorescence traces from the stopped flow analysis of halide binding to LinB wt obtained upon rapid mixing (dead time 5 ms) of 15 μM LinB with 0 – 2000 mM chloride (A), 0 – 2000 mM bromide (B) and 0 – 1000 mM iodide (C).

FIGURE 2

Dependence of amplitude of rapid equilibrium fluorescence quench on concentration of chloride (A), bromide (B) and iodide (C) for LinB wt. Solid lines represent the best fits to the data based on Stern-Volmer equation $F/F_0 = (1/(1+K_Q.[X^-])).((1+f.K_{as}.[X^-])/(1+K_{as}.[X^-]))$, in which F/F_0 is the relative fluorescence; $[X^-]$ is halide ion concentration; f is the relative fluorescence intensity of enzyme-halide complex; K_{as} is the association equilibrium constant of specific binding of halide; K_Q is the quenching constant, which is the apparent association equilibrium constant of the non-specific quenching interaction between halide and fluorophore.

FIGURE 3

Visualization of LinBwt with the p1b tunnel (in red) leading to the active site with the catalytic His272 (in green) and Asp108 with Glu132 (in red).

FIGURE 4

Free energy profiles of halides in LinBwt calculated from umbrella sampling simulations with doubly protonated (cationic) His272.

FIGURE 5

Selected important positions of iodide anion (in purple) on the way from the LinB active site to the bulk reagion (umbrella sampling simulations with catalytical His272 doubly protonated).

FIGURE 6

Free energy profiles of halides in LinBwt calculated from umbrella sampling simulations with singly protonated (neutral) His272.

FIGURE 7

Selected important positions of iodide anion (in purple) on the path from the LinB active site to the aqueous bulk (umbrella sampling simulations with His272 neutral).

FIGURE 8

Free energy profiles of sodium cation in LinBwt calculated from umbrella sampling simulations with His272 singly protonated (neutral).

FIGURE 9

Selected important positions of sodium cation (in green) on the path from the LinB active site to the aqueous bulk (umbrella sampling simulations with His272 neutral).

TABLE 1

Equilibrium constants for chloride, bromide and iodide binding to LinB.

	K_{as} (M^{-1})	K_Q (M^{-1})	f	K_d (M)	ΔG_{as} (kcal/mol)
Cl^-	3.34 ± 0.70	n.a.	0.86 ± 0.01	0.299 ± 0.063	-0.74
Br^-	4.09 ± 0.46	0.045 ± 0.032	0.53 ± 0.04	0.244 ± 0.028	-0.87
I^-	16.06 ± 0.85	0.132 ± 0.058	0.35 ± 0.02	0.062 ± 0.003	-1.71

K_{as} association equilibrium constant of specific binding

K_Q apparent association equilibrium constant of non-specific quenching interaction

f relative fluorescence intensity of enzyme-halide complex

K_d equilibrium dissociation constant for enzyme-halide complex ($K_d = 1/K_{as}$)

ΔG_{as} binding free energy (at 310.15 K)

n.a. not analysed

TABLE 2

Comparison of theoretical and experimental binding free energies of ions in the active site tunnel of LinB with the catalytic histidine in different protonation states.

	calculated ΔG_{min} His272 singly protonated *(kcal/mol)*	***experimental ΔG_{as}*** *(kcal/mol)*	***calculated ΔG_{min} His272 doubly protonated*** *(kcal/mol)*
Cl^-	-0.63	-0.74	+1.00
Br^-	-1.95	-0.87	-0.46
I^-	-2.07	-1.71	-0.49
Na^+	+1.70	-	+15.00

FIGURE 1 (graphs edited)

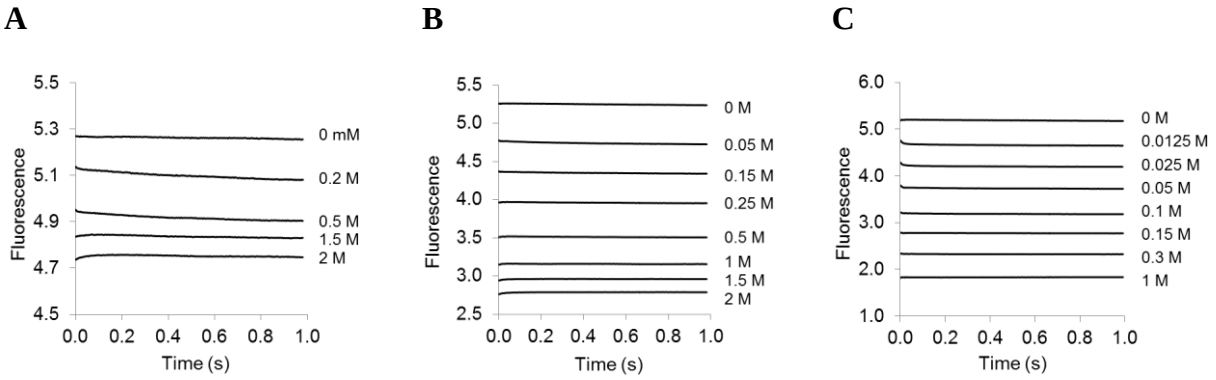

FIGURE 2 (graphs edited)

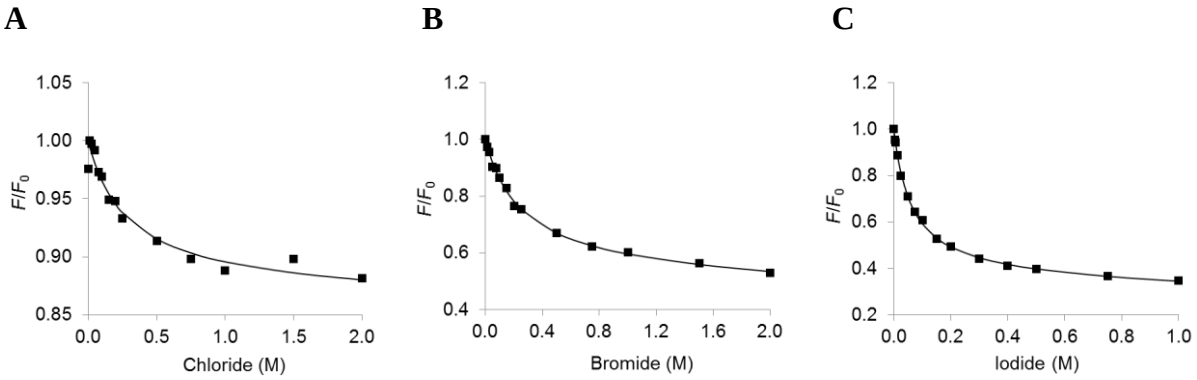

FIGURE 3

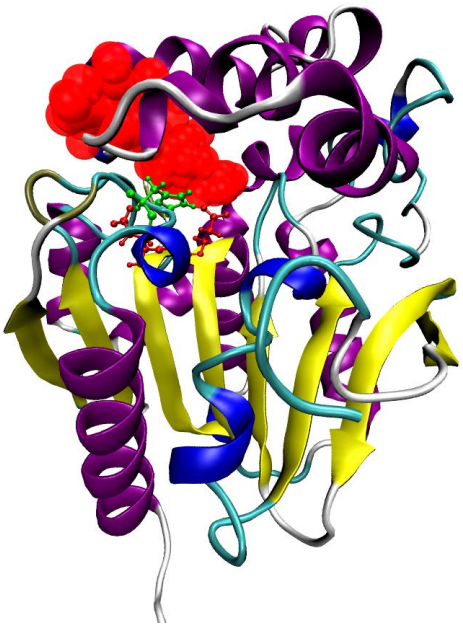

FIGURE 4

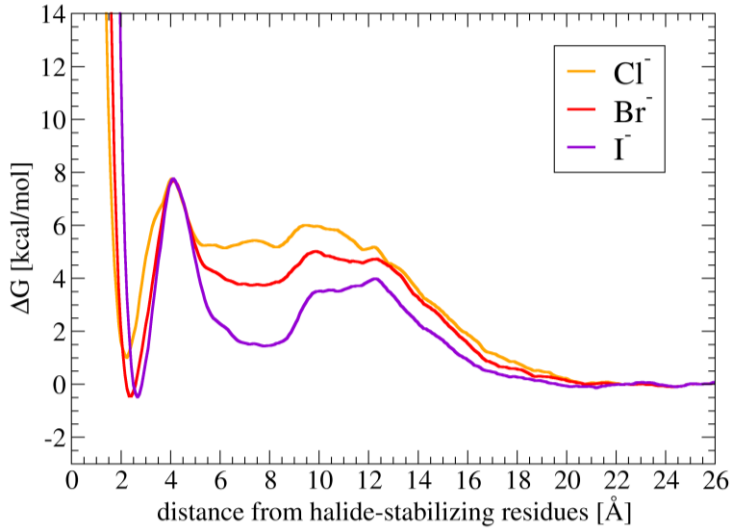
ΔG [kcal/mol]
distance from halide-stabilizing residues [Å]
Cl-
Br-
I-

FIGURE 5

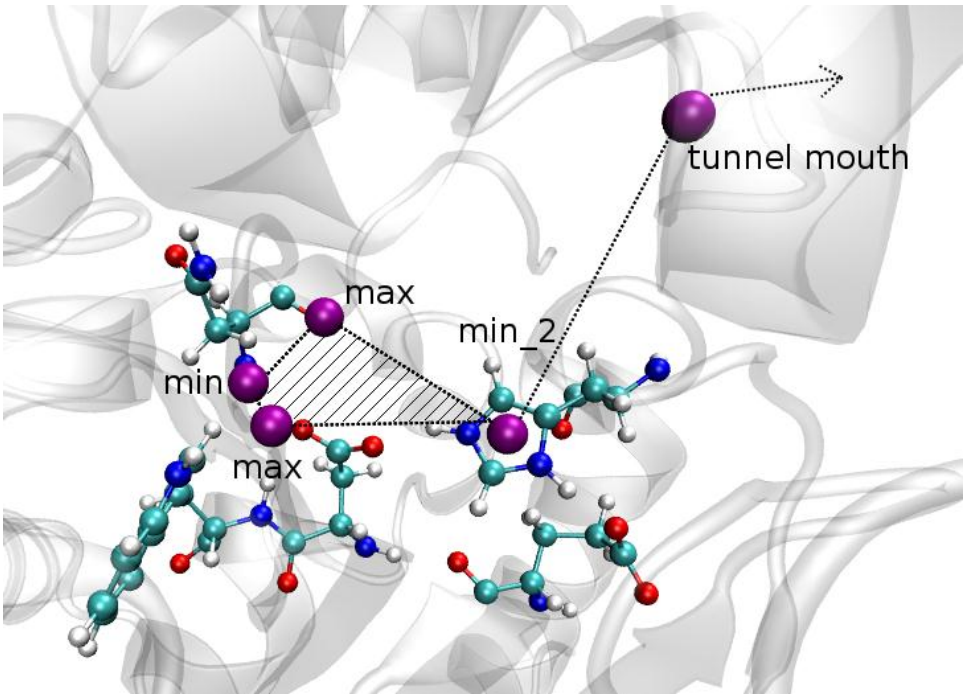

FIGURE 6

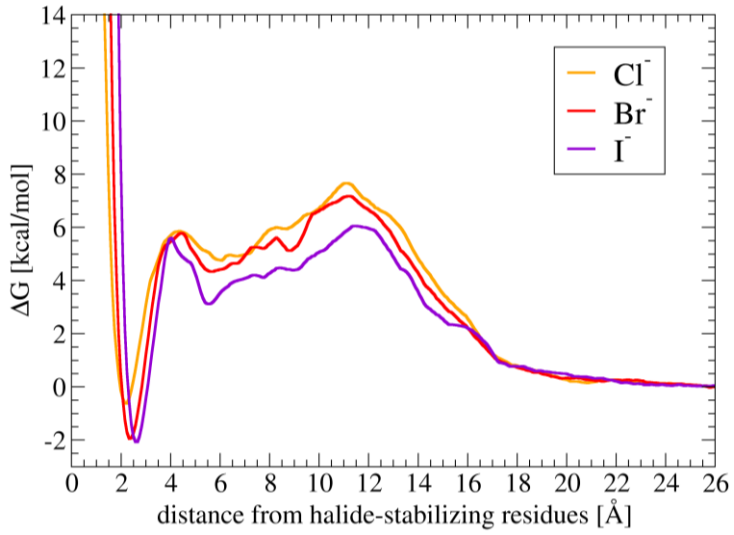
ΔG [kcal/mol]
distance from halide-stabilizing residues [Å]
Cl-
Br-
I-

FIGURE 7

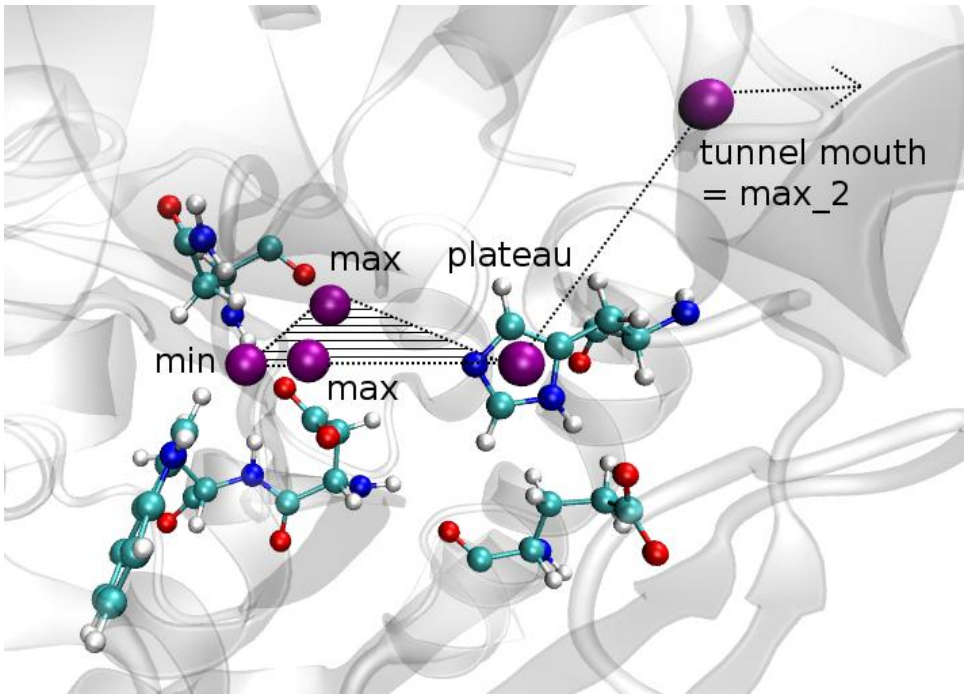

FIGURE 8

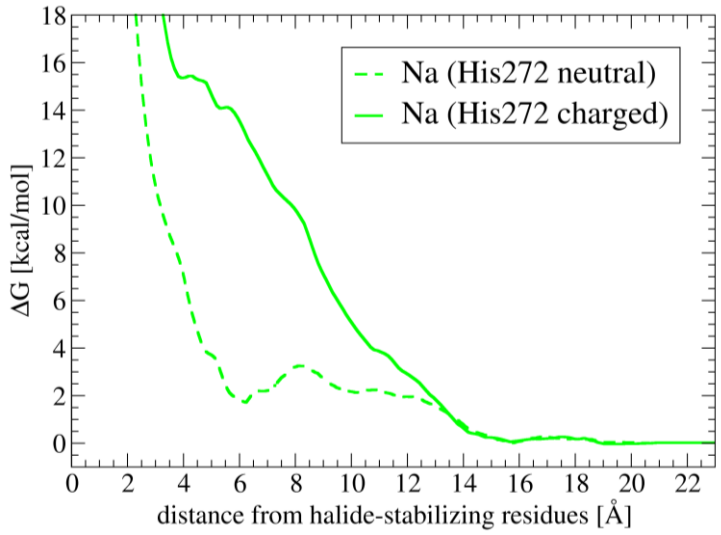
Na (His272 neutral)
Na (His272 charged)
ΔG [kcal/mol]
distance from halide-stabilizing residues [Å]
0
2
4
6
8
10
12
14
16
18
20
22

FIGURE 9

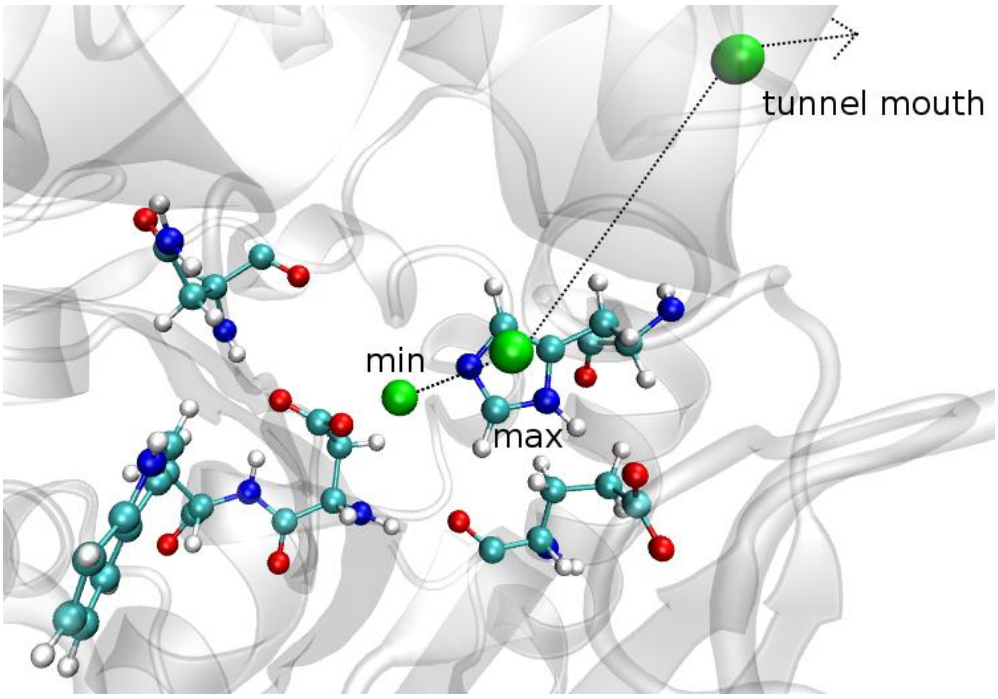

TOC Graphics.